EURASIAN PHYSICAL TECHNICAL JOURNAL

2025, Volume 22, No. 3 (53)

https://doi.org/10.31489/2025N3/36-47

Received: 19/02/2025 Revised: 19/05/2025 Accepted: 25/09/2025 Published online: 30/09/2025

Research Article

UDC 536.7; 537.311; 546.654; 549.51

THERMODYNAMIC AND ELECTROPHYSICAL PROPERTIES OF A NEW SEMICONDUCTOR BASED ON OXIDES OF RARE-EARTH AND TRANSITION METALS

Turdiyev M.T.[1], Kasenov B.K.[2*], Nukhuly A.[1], Bekturganov Zh.S.[3]
Kasenova Sh.B.[2], Sagintaeva Zh.I.[2], Kuanyshbekov E.E.[2]

[1] L.N. Gumilyov Eurasian National University, Astana, Kazakhstan
[2] Zh. Abishev Chemical-Metallurgical Institute, Karaganda, Kazakhstan
[3] E.A. Buketov Karaganda University, Karaganda, Kazakhstan
*Corresponding author: kasenov1946@mail.ru

Abstract. *The study focuses on the investigation of a new compound that combines the properties of manganites and zirconates, paving the way for the development of highly efficient functional materials. The compound was synthesized through the interaction of lanthanum oxide, zirconium oxide, manganese oxide, and sodium carbonate at temperatures ranging from 800 to 1200 °C and studied using X-ray analysis methods, including the determination of cubic lattice parameters. The analysis of the temperature dependence of heat capacity revealed second-order phase transitions, based on which equations describing its variations were derived. Thermodynamic characteristics such as entropy and enthalpy were calculated. Electrophysical measurements confirmed the semiconductor nature of the material within a specific temperature range and revealed high values of dielectric permittivity, surpassing those of reference materials.*

Keywords: manganite, lanthanum, zirconium, sodium, heat capacity, thermodynamic functions, electrophysics.

1. Introduction

Due to their magnetoresistance (MS) and colossal magnetoresistance (CMS) properties, manganites can be utilized in compact devices that respond to magnetic field variations and serve as temperature sensors and other applications [1]. Manganites can also have semiconductor, ferroelectric, para-, ferro-, and antiferromagnetic characteristics with high RAM values [1-5]. Zirconium dioxide-based compounds are extensively utilized in contemporary technologies as solid electrolytes for various electrochemical applications. Their popularity stems from exceptional properties such as high ionic conductivity, excellent chemical resistance, low thermal conductivity, and superior mechanical and optical characteristics [5–8].

The effect of adding Er_2O_3 on the electrical conductivity of c-ZrO_2 was studied by analyzing the impedance spectra of undoped and various amounts of cubic zirconium dioxide doped with Er_2O_3 (c-ZrO_2). Doped c-ZrO_2 powders and powders containing 1-15 wt.% Er_2O_3 were prepared using a colloidal method. Subsequently, the doped powders were granulated under a pressure of 200 MPa. Additionally, undoped and Er_2O_3-doped samples of c-ZrO_2 were sintered at 1500 °C for 1 hour. The electrical conductivity of the samples was measured using an impedance analyzer in the frequency range of 100 Hz to 13 MHz within a temperature range of 300-800 °C. The results indicate that the electrical conductivity increases with an increase in the test temperature. Adding 1 wt.% Er_2O_3 to c-ZrO_2 led to an increase in grain interior, grain boundary, and overall conductivity. The distortion caused by the incorporation of Er^{3+} cations into the c-ZrO_2 lattice results in an increased concentration of oxygen vacancies in c-ZrO_2 [9].

The article [10] investigates the temperature dependencies of the thermal conductivity of cubic single crystals of ZrO_2 stabilized with yttrium oxide ranging from 8 to 40 mol.% within the temperature range of 50–300 K. The cubic crystals $(ZrO_2)_{1-x}$ $(Y_2O_3)_x$, where x = 0.08–0.40, were grown using directional melt crystallization in a cold container. For x = 0.08–0.15, the thermal conductivity values are similar, and the increase in thermal conductivity with temperature is negligible. These crystals exhibit the lowest thermal conductivity within the studied concentration range. When the temperature changes from 50 to 300K, the thermal conductivity values vary from approximately 1.2–1.4 to around 2.4 W/(m·K). The differences in thermal conductivity for these compositions are noticeable only at 50 K, where the thermal conductivity of 12YSZ and 15YSZ crystals is slightly higher than that of 8YSZ, 10YSZ, and 14YSZ. The thermal conductivity of 20YSZ crystals is higher than that of crystals with yttrium oxide content in the range of x = 0.08 to 0.15, with minimal variation in conductivity over the temperature range of 50 to 300K.

Reference [11] provides a review of the thermodynamic properties of complex oxides of lanthanides and zirconium $Ln_2Zr_2O_7$ (Ln = La, Pr, Sm, Eu, Gd), as well as solid solutions of $Ln_2O_3 \cdot 2ZrO_2$ (Ln = Tb, Ho, Er, Tm). The heat capacity of $Ln_2Zr_2O_7$ samples, characterized using methods such as X-ray phase and elemental analysis, scanning electron microscopy, adiabatic and differential scanning calorimetry, is investigated. Based on the smoothed heat capacity values, the temperature dependencies of thermodynamic functions-including entropy, enthalpy changes, and reduced Gibbs energy-were determined over a broad temperature range. A comparative analysis of available thermodynamic data is presented, and recommended values are proposed. The contribution of low-temperature magnetic transitions for $Ln_2Zr_2O_7$ compounds (Ln = Pr, Nd, Sm, Gd) is taken into account, and the influence of the Schottky anomaly on the heat capacity of lanthanide compounds is explored. In study [12], the influence of the synthesis method on the microstructure of the resulting powders and ceramics of $La_{1.9}5Ca_{0.05}Zr_2O_{7-\delta}$ (LCZ) was established. In the above-mentioned and other literary sources, manganites and zirconates act as separate compounds. The article presents for the first time the compound $LaNa_2ZrMnO_6$, as combined from lanthanum (III), zirconium (IV), manganese (III) and sodium carbonate oxides to study its promising multifunctional properties.

2. Experimental technique

To synthesize the zircon-manganite $LaNa_2ZrMnO_6$, the selected starting materials included lanthanum (III) oxide ("os.ch." grade), zirconium (IV) oxide, manganese (III) oxide, and sodium carbonate ("ch.d.a." grade). Before use, these materials were dehydrated at 400 °C, then thoroughly mixed and finely ground in an agate mortar. The resulting mixture was annealed in an alund crucible within a SNOL furnace under the following conditions: initially at 600 °C for 10 hours, then at 800 °C for 10 hours, followed by 1000 °C and 1200 °C for 20 hours each. After each annealing stage, the mixture was cooled to room temperature, remixed, reground, and reheated. To prevent the formation of nonequilibrium or metastable phases at high temperatures, a final low-temperature annealing step was performed at 400 °C for 10 hours, ensuring the stability of the phase at lower temperatures [8].

The equilibrium composition of the compound was examined using X-ray phase analysis performed on a DRON-2.0 diffractometer. The analysis utilized CuK_α radiation, filtered with a Ni filter, under the following conditions: U = 30 kV, J = 10 mA, pulse counter scale set at 1000 imp/s. The counter rotation speed was set to 2 degrees per minute, with a time constant (τ) of 5 seconds. Measurements were conducted over a 2θ angle range of 10° to 90°, and the intensity of the diffraction maxima was evaluated on a 100-point scale.

The microstructural analysis of the compound was carried out using a scanning electron microscope (SEM) (Figures 1, 2). SEM image of the synthesized $LaNa_2ZrMnO_6$ at 20,000× magnification, showing agglomerated particles with irregular morphology and rough surface texture. Measurement conditions: WD = 10.75 mm, HV = 20.00 kV, HFW = 20.7 μm. Scale bar: 5 μm.

SEM image of the synthesized $LaNa_2ZrMnO_6$ at 2400× magnification, showing agglomerated particles with irregular morphology and rough surface texture. Measurement conditions: WD = 10.77 mm, HV = 20.00 kV, HFW = 173 μm. Scale bar: 50 μm.

Taken together, both images complement each other: one provides insight into the micromorphology, while the other allows for the assessment of macroscopic particle distribution and agglomeration. This combination is valuable for a comprehensive interpretation of the material's structure, particularly when discussing its functional properties such as ionic conductivity, catalytic activity, or magnetic behavior.

.

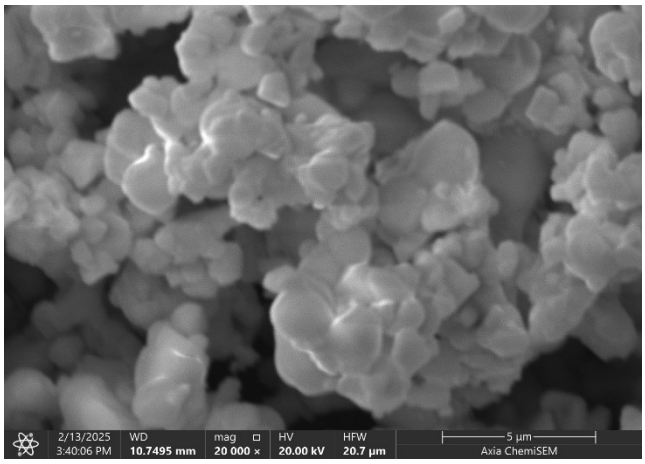

Fig. 1. Microstructure of $LaNa_2ZrMnO_6$ at a scale of 5 µm.

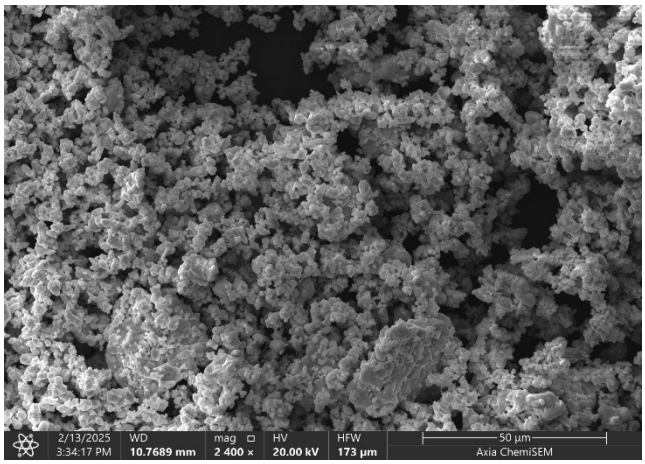

Fig. 2. Microstructure of $LaNa_2ZrMnO_6$ at a scale of 50 µm.

The isobaric heat capacity of $LaNa_2ZrMnO_6$ was investigated over the temperature range of 298–673 K using an IT-S-400 calorimeter. This instrument operates on the comparative principle of a dynamic calorimeter equipped with a heat meter. The measurement system allows temperature assessments at fixed intervals of 25 °C, utilizing a DC potentiometer and an integrated switch.

The volumetric heat capacity measurement range exceeds $1 \cdot 10^6$ J/K·m³, and the total measurement process, including experimental data processing, does not exceed 2.5 hours. The IT-S-400 calorimeter provides measurement accuracy within ±10% [8]. The device was calibrated by determining the thermal conductivity of the K_T heat meter, which represents an experimentally determined calorimeter constant [13–15]. For this purpose, experiments were performed using a copper sample and an empty ampoule. The thermal conductivity of the heat meter was calculated using the following formula [15]:

$$K_T = C_{rev.m} / (\bar{\tau}_{h.cop.} - \bar{\tau}_{h.}^{\circ}), \quad (1)$$

where $C_{rev.m}$ is the total heat capacity of the copper sample, J/(mol·K); $\bar{\tau}_{h.cop.}$ is the average delay time on the heat meter in experiments with the copper sample, s; and $\bar{\tau}_{h.}^{\circ}$ is the average delay time in experiments with an empty ampoule, s.

The total heat capacity of the copper sample was determined using the following formula [15]:

$$C_{rev.m} = C_m \cdot m_{rev}, \quad (2)$$

where C_m is the tabulated specific heat capacity of copper, J/(mol·K), and m_{rev} is the mass of the copper sample, kg.

The specific heat capacity of the substance was determined using the following formula [15]:

$$C_{spec.} = K_T / m_o(\tau_{h.} - \tau°_{h.}), \quad (3)$$

where K_T is the thermal conductivity of the heat meter, J/K; m_o is the mass of the test substance, g; $\tau_{h.}$ is the temperature delay time on the heat meter, s; and $\tau°_{h.}$ is the temperature delay time on the heat meter in experiments with an empty ampoule, s.

The molar heat capacity was obtained from the specific heat capacity by accounting for the molar mass. At each temperature, five parallel experiments were conducted, and the results were averaged and analyzed using mathematical statistical methods [15].

At each temperature, the standard deviation ($\overline{\delta}$) for the averaged values of the specific heat capacity was estimated according to [14, 15]:

$$\delta = \sqrt{\frac{\sum_{i=1}^{n}(C_i - \overline{C})^2}{n-1}}, \quad (4)$$

where n is the number of experiments, C_i is the measured value of the specific heat capacity, J/(g·K); $\overline{C}$, J/(g·K) is the arithmetic mean of the measured specific heat capacity values.

For the averaged values of the molar heat capacity, the random error component was calculated according to [14, 15] using the following formula:

$$\overset{o}{\Delta} = \frac{\delta \cdot t_p}{\overline{C}} \cdot 100, \quad (5)$$

where $\overset{o}{\Delta}$ - represents the random error component in percentage (%), and t_p is Student's coefficient. For n = 5, the value of t_p is 2.75 at a 95% confidence interval (p = 0.95) [15].

The functionality of the device was validated by measuring the heat capacity of α-Al_2O_3 (qualification "ch.d.a." in accordance with TU 6.09-426-75). Both during calibration and verification, repeated (parallel) measurements were conducted over the temperature range of 173–673K in 25K increments. At each temperature step, five parallel measurements were performed, and the results were averaged and analyzed using mathematical statistical methods [15]. To ensure the reliability of the α-Al_2O_3 heat capacity measurements, the obtained data were compared with recent literature values [16] (Table 1).

Table 1. Comparison of the measured heat capacity of α-Al_2O_3, used to verify the calorimeter's performance, with literature data [16].

T, K	$C_p°(T)$, J/(mol·K)		T, K	$C_p°(T)$, J/(mol·K)	
	Our results	By [16]		Our results	By [16]
180	44.50	43.83	400	94.12	95.21
230	64.86	61.18	450	100.26	101.8
250	70.37	67.08	500	105.47	106.1
280	77.07	74.82	550	110.09	109.7
300	76.31	79.41	600	114.29	112.5
350	86.49	88.86	650	118.20	114.9

As shown in the data presented in Table 1, our results on the temperature dependence of the heat capacity of α-Al_2O_3 within the range of 173–673K are in satisfactory agreement with the findings from [16], remaining within the accuracy limits of the IT-S-400 calorimeter. For ease of comparison, between our experimentally obtained heat capacity values for α-Al_2O_3 and the data from [16], we recalculated our results into intervals of 10 and 50 K using the equations $C°_p \sim f(T)$, derived from the experimental data. This adjustment was necessary because the data in [16] are presented in 10 and 50 K increments, while our measurements were conducted at ΔT = 25 K. It is worth noting that the actual errors in our experimental heat capacity data, determined using formulas (4, 5), are significantly smaller than the maximum device accuracy, being less than 10%. The same device was also employed for investigating the heat capacities of several compounds, as described in [17–21].

.

Tables 2 and 3, along with Figure 3, present the results obtained from the calorimetric studies and thermodynamic calculations.

Table 2. Experimentally determined heat capacity values for $LaNa_2ZrMnO_6$

T, K	$C_p \pm \overline{\delta}$, J/(g·K)	$C_p^o \pm \overset{o}{\Delta}$, J/(mol·K)	T, K	$C_p \pm \overline{\delta}$, J/(g·K)	$C_p^o \pm \overset{o}{\Delta}$, J/(mol·K)
298.15	0.5657 ± 0.0105	242 ± 12	498	0.5777 ± 0.0140	247 ± 17
323	0.7219 ± 0.0097	308 ± 11	523	0.6315 ± 0.0170	270 ± 20
348	0.7830 ± 0.0103	334 ± 12	548	0.2791 ± 0.0080	119 ± 9
373	0.8567 ± 0.0111	366 ± 13	573	0.3513 ± 0.0082	150 ± 10
398	0.9552 ± 0.0113	408 ± 13	598	0.3916 ± 0.0102	167 ± 12
423	0.7697 ± 0.0163	329 ± 19	623	0.4264 ± 0.0087	182 ±10
448	0.5649 ± 0.0055	241 ± 6	648	0.4740 ± 0.0102	202 ± 12
473	0.4338 ± 0.0077	185 ± 9	673	0.5089 ± 0.0088	217 ± 10

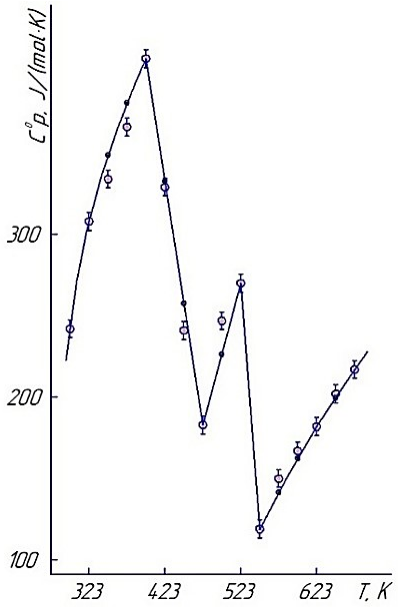

Fig. 3. Temperature dependence of the heat capacity of $LaNa_2ZrMnO_6$.
⊙ - experimental data, ● - calculated data

The electrophysical properties of $LaNa_2ZrMnO_6$ were investigated in [22] by measuring its electrical capacitance using an LCR-781, operating at a frequency of 1 kHz within a temperature range of 293-483K. According to the device specifications, the measurement accuracy for electrophysical characteristics is ±0.05% [23]. For the measurements, a plane-parallel disk-shaped sample was prepared with a diameter of 10 mm and a thickness of 5-6 mm, incorporating a binder additive. The sample was pressed under a pressure of 20 kg/cm³ and subsequently annealed in a silite furnace at 673 K for 6 hours. After annealing, the disk was ground on both sides to ensure uniformity.

The dielectric constant was calculated based on the electrical capacity of the sample. The relationship between electrical induction and the electric field strength was analyzed using the Sawyer-Tower scheme.

Table 3. Thermodynamic functions of $LaNa_2ZrMnO_6$

T, K	$C_p°(T) \pm \overset{o}{\Delta}$, J/(mol·K)	$S°(T) \pm \overset{o}{\Delta}$, J/(mol·K)	$H°(T)-H°(298.15) \pm \overset{o}{\Delta}$, J/mol	$\Phi^{xx}(T) \pm \overset{o}{\Delta}$, J/(mol·K)
298	242 ± 13	238 ± 7	–	238 ± 20
300	248 ± 13	240 ± 20	490 ± 30	238 ± 20
325	313 ± 17	262 ± 22	7540 ± 400	239 ± 20
350	358 ± 19	287 ± 24	15960 ± 850	242 ± 20
375	389 ± 21	313 ± 26	25330 ± 1350	246 ± 20
400	409 ± 22	339 ± 28	35320 ± 1880	251 ± 21
425	328 ± 17	361 ± 30	44450 ± 2370	256 ± 21
450	254 ± 14	378 ± 31	51710 ± 2760	263 ± 22
475	179 ± 10	389 ± 32	57120 ± 3040	269 ± 22
500	231 ± 12	400 ± 33	62370 ± 3320	275 ± 23
525	273 ± 15	412 ± 34	68670 ± 3660	282 ± 23
550	107 ± 6	421 ± 35	73220 ± 3900	288 ± 24
575	144 ± 8	427 ± 36	76540 ± 4080	294 ± 24
600	164 ± 9	433 ± 36	80390 ± 4280	299 ± 25
625	184 ± 10	440 ± 37	84740 ± 4510	305 ± 25
650	202 ± 11	448 ± 37	89560 ± 4770	310 ± 26
675	219 ± 12	456 ± 38	94810 ± 5050	315 ± 26

To validate the accuracy and reliability of the obtained data, the dielectric constant of barium titanate, a standard substance, was measured within the temperature range of 293–483 K at a frequency of 1 kHz.

The measured dielectric constant of $BaTiO_3$ at 293 K and 1 kHz was found to be 1296, which aligns satisfactorily with the recommended value of 1400 ± 250 [24–26]. It is worth mentioning that the electrophysical characteristics of similar manganites were also investigated using this device in studies [27, 28]. Figure 4 and Table 4 below present the results of the electrophysical studies.

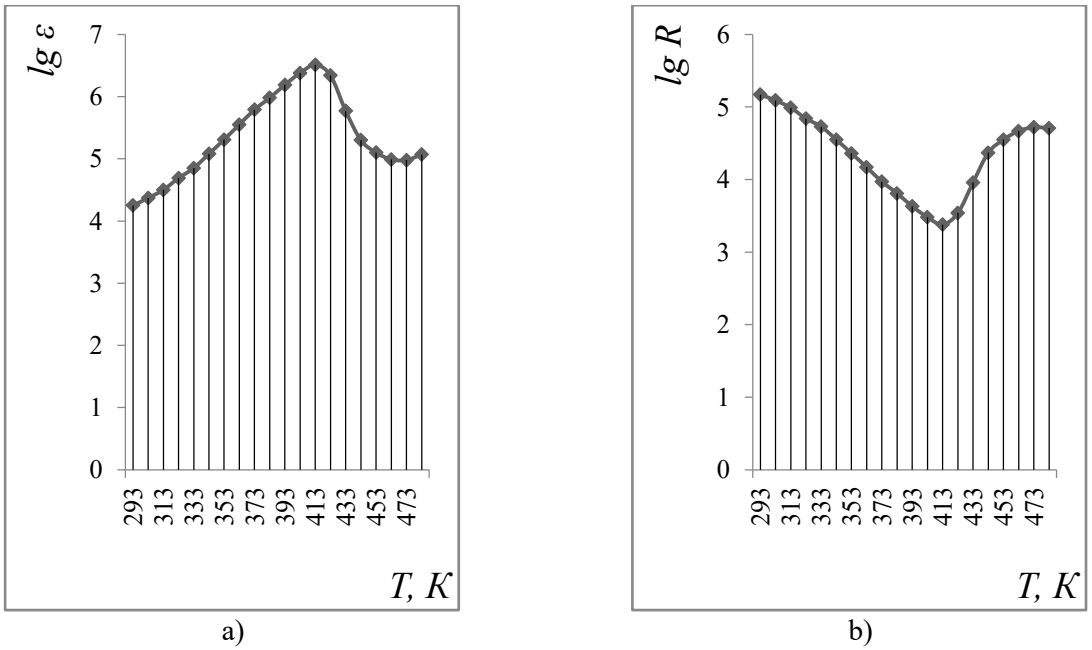

Fig. 4. Temperature dependencies of lgε (a) and lgR (b) for $LaNa_2ZrMnO_6$ (measured at a frequency of 1 kHz)

.

Table 4. The variation of electrical capacity (C), electrical resistance (R), and dielectric constant (ε) of $LaNa_2ZrMnO_6$ within the temperature range of 293–483 K at a frequency of 1 kHz

T, K	R, Ом	ε	lgε	lgR
293	148300	17819	4.25	5.17
303	121700	23188	4.37	5.09
313	96810	31849	4.50	4.99
323	69950	49343	4.69	4.84
333	53210	70768	4.85	4.73
343	35290	120019	5.08	4.55
353	22790	206349	5.31	4.36
363	14810	353176	5.55	4.17
373	9324	612617	5.79	3.97
383	6425	965360	5.98	3.81
393	4298	1561193	6.19	3.63
403	3008	2395941	6.38	3.48
413	2384	3208176	6.51	3.38
423	3474	2212127	6.34	3.54
433	9190	592580	5.77	3.96
443	23470	197557	5.30	4.37
453	35280	124671	5.10	4.55
463	46460	97860	4.99	4.67
473	52110	95612	4.98	4.72
483	51390	117508	5.07	4.71

3. Results and discussion

By analyzing the X-ray diffraction data of $LaNa_2ZrMnO_6$ using the method described in [29], it was revealed that this zircono-manganite crystallizes with a cubic symmetry. The corresponding lattice parameters are as follows: a = 16.85 ± 0.02 Å; V^0 = 4785.46 ± 0.02 Å^3; Z = 6; $V°_{elem\ cell}$ = 795.58 ± 0.02 Å^3; $\rho_{x\text{-}ray.}$ = 5.35 g/cm^3; and $\rho_{picn.}$ = 5.30 ± 0.04 g/cm^3 [30].

The pycnometric density was determined according to [31]. Toluene was used as an indifferent liquid.

Based on the calorimetric studies presented in Fig. 3 and Table 2, $LaNa_2ZrMnO_6$ exhibits distinct anomalies in its heat capacity at temperatures of approximately 300 K and 523 K. These discontinuities in the heat capacity curve ($C°_p \sim f(T)$) likely indicate second-order phase transitions. Such transitions may be influenced by factors such as Schottky effects, variations in magnetoresistance, electrical resistance, and permittivity, potentially associated with Curie and Néel points [32, 33], as well as other contributing phenomena [34]. Considering the temperatures at which these phase transitions occur, the equations describing the temperature dependence of the heat capacity of $LaNa_2ZrMnO_6$ have been derived and are expressed as the following polynomials (J/(mol·K)):

$$C^0_{p(1)} = (1235 \pm 66) - (1169.6 \pm 62.3)\cdot 10^{-3}T - (572.5 \pm 30.5)\cdot 10^5 T^{-2} \text{ (298-398 K)}, \quad (6)$$

$$C^0_{p(2)} = (1589 \pm 85) - (2968.7 \pm 158.2)\cdot 10^{-3}T \quad \text{(398-473 K)}, \quad (7)$$

$$C^0_{p(3)} = -(619 \pm 33) + (1688.4 \pm 90.0)\cdot 10^{-3}T \quad \text{(623-673 K)}. \quad (8)$$

$$C^0_{p(4)} = (3418 \pm 182) - (6020.0 \pm 320.9)\cdot 10^{-3}T \quad \text{(523-548 K)}, \quad (9)$$

$$C^0_{p(5)} = (104 \pm 5.6) - (333.9 \pm 17.8)\cdot 10^{-3}T - (502.8 \pm 26.8)\cdot 10^5 T^{-2} \quad \text{(548 – 673 K)}, \quad (10)$$

Due to the limitations of the calorimeter's technical specifications, the standard entropy of $LaNa_2ZrMnO_6$ was determined by estimating ionic entropy increments: La^{3+} (40.4), Na^+ (34.6), Zr^{4+} (23.6), Mn^{3+} (34.7), and O^{2-} (11.7) J/(mol·K) [35].

These values were applied according to the following scheme:

$$S^{o}(298.15)\ LaNa_2ZrMnO_6 = S^{i}(298.15)\ La^{3+} + 2S^{i}(298.15)\ Na^{+} + \\ + S^{i}(298.15)\ Zr^{4+} + S^{i}(298.15)\ Mn^{3+} + 6S^{i}(298.15)\ O^{2-}, \quad (11)$$

where $S^{i}(298.15)$ – entropic increments of ions entropic increments of ions.

The standard entropy of $LaNa_2ZrMnO_6$, calculated according to scheme (11) is 238 ± 7 J/(mol·K). The standard heat capacity of $LaNa_2ZrMnO_6$ was determined using an independent method based on ionic increments of heat capacity [35]. The input values for $C^{i}_{p}(298.15)$ were as follows: La^{3+} = 29.3, Na^{+} = 26.8, Zr^{4+} = 22.9, Mn^{3+} = 25.0, and O^{2-} = 16.7 J/(mol·K). The calculated heat capacity was found to be 231.0 J/(mol·K), which aligns well with the experimental result of 242 ± 12 J/(mol·K), showing a deviation of only 4.8%.

Using experimental heat capacity data and the calculated standard entropy values at 25 K increments, the temperature dependencies of $C^{\circ}_{p}(T)$ and the thermodynamic functions S°(T), H°(T) - H°(298.15), and Φ^{xx}(T) were determined. The activation energy of electrical conductivity (ΔE) was determined by utilizing the following approach: Experimental values of temperature (T) and resistance (R) were plotted as a dot chart with markers. An exponential trend line was then added to the graph to verify that the experimental data aligns with a function of the form:

$$R_{nn} = R_0 e^{\frac{\Delta E}{2KT}}. \quad (12)$$

Using the least squares method and linear regression, we will construct a dot diagram of the dependence of lgR_{nn} от 10^4/T based on experimental data. Next, we add a linear trend line or create a system of equations: lgy = a + bx, где y = lg R, x = 10^4/T (Figure 5).

We obtain for $LaNa_2ZrMnO_6$ in the range 293-413 K the dependence lgR~f(1/T) (Figure 4a), which is described by the equation:

$$y = -1.2139 + \frac{1932}{T} \quad (13)$$

and let's compare it with the shape:

$$lgR_n = \frac{\Delta E}{2K} \cdot T + lgR, \quad (14)$$

then $\frac{\Delta E}{2K} = 1932K$, lgR_0=-1.2139 from where:

$$\Delta Ea = \frac{1932 \cdot 2 \cdot 1.38 \cdot 10^{-23}}{1.6 \cdot 10^{-19}} = 0.333\ eV, \quad (15)$$

where k = 1.38·10^{-23} Дж·K^{-1} – Boltzmann's constant, e = 1.6·10^{-19} KL – elementary charge.

The band gap width (ΔE_g) of the test substance was calculated using the formula:

$$\Delta E_g = \frac{2k\ T_1 T_2}{0.43(T_2 - T_1)} lg \frac{R_1}{R_2}, \quad (16)$$

where k - Boltzmann's constant, equal to 8.617302·10^5 eV. K^{-1}, R_1 – resistance at T_1, R_2 - resistance at T_2.

$$\Delta E_g = \frac{2 \cdot 0.000086173 \cdot 293 \cdot 413}{0.43(413 - 293)} \cdot \frac{5.17}{4.71} = 0.44\ eV. \quad (17)$$

The $LaNa_2ZrMnO_6$ compound in the range of 293-413 K has a band gap of 0.44 eV. The activation energy shows how much energy is required to transfer charge carriers (electrons or holes) in a material A value of 0.333 eV indicates that at room temperature (293 K) and above, the $LaNa_2ZrMnO_6$ material has a moderate energy required to activate conduction. This value helps to understand how easily a material can conduct electric current when heated. The band gap width determines the energy gap between the valence and conductive zones in the material. A value of 0.44 eV indicates that $LaNa_2ZrMnO_6$ is a semiconductor with a narrow band gap. Materials with these characteristics can be used in a variety of applications, including thermal sensors and devices operating at low temperatures.

.

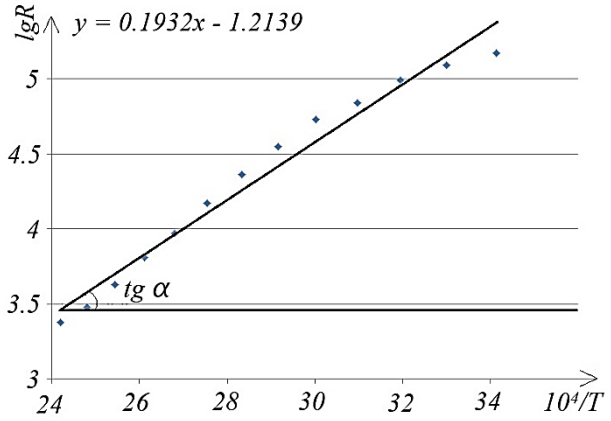

Fig. 5. Linear dependence of lg R ~ 10^4/T in the range - 293-413 K α

Electrophysical studies reveal that the material demonstrates semiconductor conductivity within the temperature range of 293–413 K. Beyond this range, from 413 to 473 K, it transitions to metallic conductivity. The dielectric constant of this zircono-manganite at 293 K and a frequency of 1 kHz is 14 times higher than that of the standard $BaTiO_3$ (1296), and 54 times higher at 483 K ($BaTiO_3$, ε = 2159) ($LaNa_2ZrMnO_6$, ε = 117508). At the transition temperature of 413 K, where the material shifts from semiconductor to metallic conductivity, the highest value of ε is observed at 3208176. This remarkable value surpasses the dielectric constant of the reference material $BaTiO_3$ at the same temperature (1626) by an impressive factor of 1973, highlighting the material's exceptional dielectric properties in this range.

The conduction mechanism for La and Zr in $LaNa_2ZrMnO_6$.

When La and Zr atoms are partially replaced, lanthanum and zirconium atoms can interact with other elements in the crystal lattice, creating unique energy levels. In this case, the conduction mechanism may look like this. La and Zr atoms have different charge states that affect the conductivity of the material. For example, the La atom may be in the La^{3+} state, and the Zr atom in the Zr^{4+} state. La and Zr atoms can create acceptor levels inside the band gap. These levels will be close to the valence band and separated by an energy gap that determines the activation energy.

When the bonds between atoms are heated and weakened, new covalent bonds can form. An electron can move from one atom to another, forming additional covalent bonds. Such a transition requires energy ΔE_a, which can be significantly less than the energy ΔE required for the transition of an electron into the conduction band.

When an electron leaves an atom and moves to another, the atom from which the electron left forms a hole. In the case of substitution of La and Zr atoms, they can serve as acceptors, and the holes they create will be located inside the band gap.

When an external electric field is applied, the holes in the valence band move due to the abrupt transition of electrons. This leads to p-type conductivity, in which holes are the main charge carriers. Thus, with partial substitution of La and Zr atoms, a conduction mechanism associated with the formation of acceptor levels and hole conduction is possible. The above studies show that this compound is of interest for semiconductor technology and as a RAM material.

4. Conclusions

1. $LaNa_2ZrMnO_6$ zircono-manganites, which crystallizes in cubic syngony, were synthesized for the first time by high-temperature synthesis.
2. The temperature dependence of the heat capacity of $LaNa_2ZrMnO_6$ was investigated using dynamic calorimetry over the temperature range of 298-673 K.
3. It was found that the $C^\circ_p \sim f(T)$ curve exhibits anomalous jumps in heat capacity at 398 K and 523 K, likely corresponding to second-order phase transitions, which indicate the presence of valuable physicochemical properties.

4. Taking into account the phase transition temperatures, the equations describing the temperature dependence of heat capacity have been calculated.

5. Fundamental values have been determined, including the experimental standard heat capacity and the calculated standard entropy of $LaNa_2ZrMnO_6$.

6. Based on the experimental $C°_p(T)$ data and the estimated S°(298.15) values at 25 K intervals, the temperature dependence of $C°_p(T)$ and the thermodynamic functions S°(T), H°(T) - H°(298.15), and Φ^{xx}(T) were calculated.

7. The band gap and activation energies of $LaNa_2ZrMnO_6$ conductivity are calculated and it is established that this semiconductor can be classified as a p- type semiconductor.

8. Electrophysical studies have shown that $LaNa_2ZrMnO_6$ is of interest for semiconductor technology with high RAM values.

9. The research results are valuable for the targeted synthesis of similar compounds with tailored properties, physicochemical modeling of processes involving the studied compound, and applications in the chemistry and technology of semiconductor materials. Additionally, the obtained data serve as source information for uploading fundamental thermodynamic constants into databases.

Conflict of interest statement

The authors declare that they have no conflict of interest in relation to this research, whether financial, personal, authorship or otherwise, that could affect the research and its results presented in this paper.

CRediT author statement

Turdiyev M.T., Kasenov B.K., Nukhuly A.: conceptualization, methodology, writing – review and editing; **Bekturganov Zh.S., Kasenova Sh.B.:** formal analysis, writing – original draft preparation; **Sagintaeva Zh.I., Kuanyshbekov E.E.:** investigation, writing – original draft preparation. The final manuscript was read and approved by all authors.

References

1 Karpasyuk V.K., Smirnov A.M., Badelin A.G. (2015) Features of constructing magnetic field sensors based on the colossal magnetoresistance effect. *Caspian Journal: Management and High Technologies*, 4, 291 – 297. [in Russian]. Available at: https://hi-tech.asu-edu.ru/files/4(32)/291-297.pdf

2 Menglei Li, Hengxin Tan, Wenhui Duan (2020) Hexagonal rare-earth manganites and ferrites: a review of improper ferroelectricity, magnetoelectric coupling, and unusual domain walls. *Phys. Chem. Chem. Phys.*, 22, 14415 – 14432. https://doi.org/10.1039/D0CP02195D

3 Yang Shen, Ce-Wen Nan. (2023) High thermal conductivity dielectric polymers show record high capacitive performance at high temperatures. *National Science Review*, 10 (11), nwad224. https://doi.org/10.1093/nsr/nwad224

4 Chabushkin A.N., Lyapin A.A., Ryabochkina P.A., Antipov O.L., Artemov S.A., Lomonova E.E. (2018) CW and Q-switched 2 m solid-state laser on ZrO_2–Y_2O_3–HO crystals pumped by a Tm fiber laser. *Laser Phys*, 28 (3), 035803. https://doi.org/10.1088/1555-6611/aa962f

5 Zhirenkina N.V. (2022) Technology of Powder Synthesis Based on Zirconium Dioxide for the Production of High-Density Ceramics. 2.6.14. Technology of Silicate and Refractory Nonmetallic Materials. Dissertation for the Degree of Candidate of Technical Sciences. Yekaterinburg, 159.

6 Arachi Y., Sakai H., Yamamoto O., Takeda Y., Imanishai N. (1999) Electrical conductivity of the ZrO_2–Ln_2O_3 (Ln=lanthanides) system. *Solid State Ionics*, 121, 1-4, 133 –139. https://doi.org/10.1016/s0167-2738(98)00540-2

7 Borik M.A, Bublik V.T., Kulebyakin A.V., Lomonova E.E., Milovich F.O., Myzina V.A., Osiko V.V., Tabachkova N.Y. (2014) Phase composition, structure and mechanical properties of PSZ (partially stabilized zirconia) crystals as a function of stabilizing impurity content. *Alloys and Compounds,* 586, 231 – 235. https://doi.org/10.1016/j.jallcom.2013.01.126

8 Zadorozhnaya O.Y., Napochatov Y.K., Agarkova E.A., Tiunova O.V. (2020) Layered sold-electrolyte membranes based on zirconia: production technology. *Russian Journal of Electrochemistry*, 56 (2), 124 – 131. https://doi.org/10.1134/S1023193520020123

9 Aktas B., Tekeli S., Kucuktuvek M. (2014) Electrical Conductivity of Er_2O_3-Doped c-ZrO_2 Ceramics. *J. of Materi Eng and Perform*, 23, 349–355. https://doi.org/10.1007/s11665-013-0750-5

10 Borik M.A., Volkova T.V., Kulebyakin A.V., Kuritsyna I.E., Lomonova E.E., Myzina V.A., Milovich F.O., Ryabochkina P.A., Tabachkova N.Yu., Zentsova A.I., Popov P.A. (2020) Thermal Conductivity of Cubic ZrO_2 Single Crystals Stabilized with Yttrium Oxide. *Physics of the Solid State*, 62, 1, 235 – 239. https://doi.org/10.1134/s1063783420010072

.

11 Guskov V.N. Gavrichev K.S. Gagarin P.G., Guskov A.V. (2019) Thermodynamic Functions of Complex Zirconia Based Lanthanide Oxides-Pyrochlores $Ln_2Zr_2O_7$ (Ln = La, Pr, Sm, Eu, Gd) and Fluorites $Ln_2O_3 \cdot 2ZrO_2$ (Ln = Tb, Ho, Er, Tm). *Russ. J. Inorg. Chem*, 64, 10, 1265 - 1281. https://doi.org/10.1134/S0036023619100048

12 Stroeva A.Yu., Vorotnikov V.A., Bervitskaya O.S., Ichetovkina V.A., Ichetovkin Z.N., Duvakin A.M., Ananchenko B.A., Kuzmin A.V. (2024) The effect of synthesis technique on the microstructure of doped lanthanum zirconate materials. *Electrochemical Energetics*, 24, 4, 185 - 190. [in Russian]. https://doi.org/10.18500/1608-4039-2024-24-4-185-190

13 Proshkin S. (2018) Multipurpose calorimeter to measure thermophysical properties ARPN *Journal of Engineering and Applied Science*s, 2018, 13, 5, 1827 – 1832.

14 Bychinskii V.A., Tupitsyn A.A., Mukhetdinova A.V., Chudnenko K.V., Fomichev S.V., Krenev V.A. (2013) Estimation of the heat capacity of individual substances on the basis of experimental enthalpy increments. *Russian Journal of Inorganic Chemistry*, 58(9), 1079 – 1084. https://doi.org/10.1134/s0036023613090040

15 Rustembekov K.T., Sharipova Z.M., Dyusekeeva A.T. (2012) Thermochemistry of selenates of some s- d-elements. *Journal of international Scientific Publications: Materials, Methods & Technologies*, 6, 286 - 295. Available at: https://www.scientific-publications.net/download/materials-methods-and-technologies-2012-2.pdf

16 Bodryakov V.Yu., Bykov A.A. (2015) Correlation characteristics of the temperature coefficient of volumetric expansion and heat capacity of corundum. *Glass and ceramics*, 2, 30. [in Russian]. https://doi.org/10.1007/s10717-015-9726-2

17 Kassenov B.K., Kassenova Sh.B., Sagintaeva Zh.I., Kuanyshbekov E.E., Turtubaeva M.O. (2020) Calorimetric Research into the Heat Capacity of Novel Nano-sized Cobalt(Nickelite)-Cuprate-Manganites of $LaBaMe^{II}CuMnO_6$ (Me^{II}= Co, Ni) and their Thermodynamic Properties. *Eurasian Chemico-Technological Journal*, 22, 27 – 33. https://doi.org/10.18321/ectj927

18 Rustembekov K.T., Kasymova M.S., Kaikenov D.A., Fomin V.N., Aldabergenova S.K., Toybek A.A. (2019) Calorimetry of new double dysprosium tellurite. *Bulletin of Karaganda university. Chemistry series,* 93, 1, 60 – 65. https://doi.org/10.31489/2019ch1/60-65

19 Kasenova Sh.B., Sagintaeva Zh.I., Kasenov B.K., Ermaganbetov K.T., Kuanyshbekov E.E., Seisenova A.A., Smagulova D.I. (2013) Calorimetry and thermodynamic properties of nanostructured cuprate-manganite of lanthanum and strontium $LaSr_2CuMnO_6$. *News of NAS RK. Chemical sciences series,* 401, 5, 85 - 89. [in Russian]. Available at: https://nauka.kz/page.php?page_id=964&new&page=7845

20 Kasenov B.K., Kasenova Sh. B., Sagintaeva Zh.I., Kuanyshbekov E.E., Nuhuly A. Heat capacity of the new nano-size cobalt-cuprato-manganite $LaLi_2CoCuMnO_6$ in the interval of 298.15-673 K and its thermodynamic properties. *Applied solid state Chemistry,* 2018, 5 (4), 82-85. https://doi.org/10.18572/2619-0141-2018-4-5-82-85

21 Rustembekov K., Dyusekeyeva A., Sharipova Z., Amanzhan A. (2012) Syntesis and thermochemistry of new metal-mixed tellurites. *Chemical Bulletin of Kazakh National University*, 65(1), 170-174. https://doi.org/10.15328/chemb_2012_1170-174

22 Kasenov B., Kasenova S., Sagintaeva Z., Kuanyshbekov E., Bekturganov Z., Zeynidenov A. (2022) Electrophysical properties of new nanostuctured copper-zinc manganite of lanthanum and magnesium. *Eurasian Physical Technical Journal*, 2022, *19*(2(40), 42–47. https://doi.org/10.31489/2022No2/42-47

23 *Operation Manual. RLC meter (LCR-781)*. Moscow: PriST CJSC, 2012, 3 [in Russian]. Available at: https://prist.ru/upload/iblock/5a9/zv6bz0pv1oji5hdghyqzf8jwi26uaizw/Izmeritel-LCR_78200_5-mod._.pdf

24 Al Jaafari F.M.D., Korotkov L.N., Tolstykh N.A., Emelianov N.A., Pankova M.A., Popov S.V. (2023) Dielectric properties of mixed $BaTiO_3$–$SrTiO_3$ nanocomposites. *Bulletin of the Russian Academy of Sciences: Physics,* 87, 9, 1302 - 1307. https://doi.org/10.3103/S1062873823703197

25 Dikov R.V. (2022) Study of the Electrophysical Properties of Ferroelectric Piezo-Ceramics Based on Barium Titanate. Dissertation for the Degree of Candidate of Physical and Mathematical Sciences. 1.3.5. *Physical Electronics*. Volgograd, 128. [in Russian]. Available at: https://www.vstu.ru/upload/iblock/67e/67e5be44aa5e9d2ed1fecbb761609f3a.pdf

26 Wang J.J., Meng F.Y., Ma X.Q., Xu M.X., Chen L.Q. (2010) Lattice, elastic, polarization, and electrostrictive properties of $BaTiO_3$ from first-principles *J. Appl. Phys.* 108, 034107. https://doi.org/10.1063/1.3462441

27 Mataev M., Madiyarova A., Patrin G., Abdraimova M., Nurbekova M. Durmenbayeva Zh. (2024) Synthesis of New Complex Ferrite $Li_{0.5}MnFe_{1.5}O_4$: Chemical-Physical and Electrophysical Research, *Materials,* 17, 3754. https://doi.org/10.3390/ma17153754

28 Kasenov B.K., Kasenova Sh.B., Sagintaeva Zh.I., Kuanyshbekov E.E., Mukhtar A.A. (2022) Thermodynamic and Electrophysics of New $LaCaCuZnMnO_6$ Copper – Zinc Manganite of Lanthanum and Calcium. *High Temperature*, 60, 4, 474 - 478. https://doi.org/10.1134/S0018151X22020225

29 Guo G., Goldfeder J., Lan L., Ray A., Hanming Yang A., Chen B., J. L. Billinge S., Lipson H. (2024) Towards end-to-end structure determination from x-ray diffraction data using deep learning. *npj Comput Mater*, 10, 209. https://doi.org/10.1038/s41524-024-01401-8

30 Turdiyev M.T., Kasenov B.K., Nukhuly A., Stoev M., Sagintaeva Zh.I., Kasenova Sh.B., Kuanyshbekov E.E. (2024) New zircon-manganites of lanthanum and alkali metals. *Chemical Bulletin of Kazakh National University,* 111, 1-2, 23 - 27. https://doi.org/10.15328/cb1372

31 Viana, M,. Jouannin P., Pontier C., Chulia D. (2002) About pycnometric density measurements. *Talanta*, 57(3), 583 – 593. https://doi.org/10.1016/S0039-9140(02)00058-9

32 Hemminger W., Höhne G. (1984) *Calorimetry: Fundamentals and Practice.* Weinheim: Verlag Chemie, 310 p.

33 Goldenfeld N. *Lectures on Phase Transitions and the Renormalization Group*. CRC Press, Taylor & Francis Group, 1992. eBook published 2018. 420 p. https://doi.org/10.1201/9780429493492

34 Xue Y., Shen Z., Wu Z., Song C. (2023) Thickness dependence of the critical temperature and magnetic coupling in multilayer $Cr_2Sn_2Te_6$. *Physical Review B*., 108, 064416. https://doi.org/10.1103/PhysRevB.108.064416

35 Melchakova O.V., Zaitseva P.V., Mayorova A.V., Kulikova T.V., Pechishcheva N.V., Shunyaev K.Yu. (2019) Calculation of the Thermodynamic Properties of Metal Perrhenates and Their Use in Modeling Sample Preparation for Chemical Analysis. *Analytics and Control,* 23, 4, 570 – 579. https://doi.org/10.15826/analitika.2019.23.4.015 [in Russian].

AUTHORS' INFORMATION

Turdiyev, Myktybek Tolkynbayuly – PhD student, Master, L.N. Gumilyov Eurasian National University, Astana, Kazakhstan, https://orcid.org/0009-0007-0187-6804; turdiev.miktibek@gmail.com

Kasenov, Bulat Kunurovich – Doctor of chemical sciences, Professor, Head of the Laboratory of thermochemical processes, Abishev Chemical-Metallurgical Institute, Karaganda, Kazakhstan; https://doi.org/0000-0001-9394-0592; kasenov1946@mail.ru

Nukhuly, Altynbek – Doctor of chemical sciences, Professor, L.N. Gumilyov Eurasian National University, Astana, Kazakhstan; https://doi.org/0000-0001-5006-879X; nukhuly@mail.ru

Bekturganov, Zhanaly Sultanovich – Doctor of chemical sciences, Professor, Department of radiophysics and electronics, E.A. Buketov Karaganda University, Karaganda, Kazakhstan; https://doi.org/0000-0002-6487-7835; zhbekturganov@gmail.com

Kasenova, Shuga Bulatovna – Doctor of chemical sciences, Professor, Chief researcher, Laboratory of thermochemical processes, Abishev Chemical-Metallurgical Institute, Karaganda, Kazakhstan; https://doi.org/0000-0001-9755-7478; kasenovashuga@mail.ru

Sagintaeva, Zhenisgul Imangalievna – Candidate of chemical sciences, Associate Professor, Leading Researcher, Laboratory of thermochemical processes, Abishev Chemical-Metallurgical Institute, Karaganda, Kazakhstan; https://doi.org/0000-0001-8655-356X; kai_sagintaeva@mail.ru

Kuanyshbekov, Erbolat Ermekovich – Master (Eng.), Senior Researcher, Laboratory of thermochemical processes, Abishev Chemical-Metallurgical Institute, Karaganda, Kazakhstan; https://doi.org/0000-0001-9172-9566, mr.ero1986@mail.ru

.